DOI: 10.1002/chem.200600063

Substituent Effects on the Stereochemistry of Gas-Phase Intracomplex Nucleophilic Substitutions

Antonello Filippi,[a] Caterina Fraschetti,[a] Gabriele Renzi,[b] Graziella Roselli,[b] and Maurizio Speranza*[a]

Abstract: The mechanism and stereochemistry of the intracomplex solvolysis of proton-bound complexes $[\mathbf{Y}\cdots H\cdots\mathbf{M}]^+$ between $\mathbf{M} = CH_3{}^{18}OH$ and $\mathbf{Y}$ = 1-arylethanol [(*S*)-1-(*para*-tolyl)ethanol ($\mathbf{1}_S$), (*S*)-1-(*para*-chlorophenyl)ethanol ($\mathbf{2}_S$), (*S*)-1-(*meta*-α,α,α-trifluoromethylphenyl)ethanol ($\mathbf{3}_S$), (*S*)-1-(*para*-α,α,α-trifluoromethylphenyl)-ethanol ($\mathbf{4}_S$), (*R*)-1-(pentafluorophenyl)-ethanol ($\mathbf{5}_R$), (*R*)-α-(trifluoromethyl)-benzyl alcohol ($\mathbf{6}_R$), and (*R*)-1-phenylethanol ($\mathbf{7}_R$)] have been investigated in the gas phase (CH_3F; 720 Torr) in the 25–140 °C temperature range. Gas-phase solvolysis of $[\mathbf{Y}\cdots H\cdots\mathbf{M}]^+$ ($\mathbf{Y} = \mathbf{2}_S$, $\mathbf{3}_S$, $\mathbf{4}_S$, and $\mathbf{7}_R$) leads to extensive racemization above a characteristic temperature $t^{\#}$ (e.g. at $t^{\#} > 60$ °C for $\mathbf{7}_R$), whereas below that temperature the reaction displays a preferential retention of configuration. Predominant retention of configuration is instead observed in the intracomplex solvolysis of $[\mathbf{Y}\cdots H\cdots\mathbf{M}]^+$ ($\mathbf{Y} = \mathbf{1}_S$, $\mathbf{4}_S$, $\mathbf{5}_R$, and $\mathbf{6}_R$) with the temperature range investigated ($25 \leq T \leq 120$ °C). These results indicate that the intracomplex solvolysis proceeds through the intermediacy of the relevant benzylic cations (Bz^+), which is electrostatically coordinated to a H_2O and a $CH_3{}^{18}OH$ molecule (a pure S_N1 mechanism). The obtained gas-phase mechanism is discussed in the light of related solution data. It is concluded that the stereochemistry of unimolecular solvolytic reactions is determined by the lifetime and the dynamics of the species involved and, if occurring in solution, by the nature and the dynamics of the solvent cage as well.

Keywords: chirality · gas-phase reactions · kinetics · nucleophilic substitution

Introduction

The mechanism of solvolytic reactions involving the intermediacy of a free carbocation (S_N1) has been the matter of intense investigation during the last century.[1,2] Despite such a considerable effort, the modeling of S_N1 processes remains difficult because of the lack of a sufficiently detailed knowledge of the dynamics of the relevant ion–dipole or ion–counterion intermediates generated in the solvent cage. Indeed, the presence itself of the solvent cage may affect the behaviour of the active S_N1 transients, since transport (diffusion) and solvation phenomena may prevail over intrinsic reactivity factors.[3–8] For these reasons, it would be an advantage to study simplified examples of these reactions. The ideal would be to dissect the solvolytic process into its components both with regard to the interaction with the solvent molecules and the identification of the sequence of the elementary steps.

In many respects, the gas phase provides an ideal environment for studying elementary solvolytic reactions involving a single solvent molecule in the absence of bulk solvation and diffusion phenomena.[9] Recently, the kinetics and stereochemistry of the evolution of proton-bound adducts between $CH_3{}^{18}OH$ and the 1-arylethanols $[\mathbf{Y}\cdots H\cdots\mathbf{M}]^+$ [$\mathbf{M}$ = (*R*)-1-(pentafluorophenyl)ethanol ($\mathbf{5}_R$) and (*R*)-1-phenylethanol ($\mathbf{7}_R$); Scheme 1] have been investigated in detail in gaseous CH_3F at 720 Torr and at temperatures from 25 to 100 °C.[10] The noncovalent $[\mathbf{Y}\cdots H\cdots\mathbf{M}]^+$ adducts were obtained in the gas phase by association of the relevant chiral alcohol ($\mathbf{Y}$ in Scheme 1) with the $CH_3{}^{18}OH_2{}^+$ ion, generated by γ radiolysis of $CH_3F/H_2{}^{18}O$ mixtures (left-handed inset in Scheme 1).[11] This approach allows formation of $[\mathbf{Y}\cdots H\cdots\mathbf{M}]^+$ in a gaseous inert medium (CH_3F) at pressures high enough (720 Torr) to ensure its complete thermaliza-

[a] Dr. A. Filippi, Dr. C. Fraschetti, Prof. M. Speranza
Dipartimento degli Studi di Chimica e Tecnologia delle Sostanze Biologicamente Attive
Università "La Sapienza", 00185 Roma (Italy)
Fax: (+39) 06-49913602
E-mail: maurizio.speranza@uniroma1.it

[b] Prof. G. Renzi, Dr. G. Roselli
Dipartimento di Scienze Chimiche
Università degli Studi di Camerino
V.S. Agostino 1, 62032 Camerino (Mc) (Italy)

Pagination corrected Oct. 17, 2006

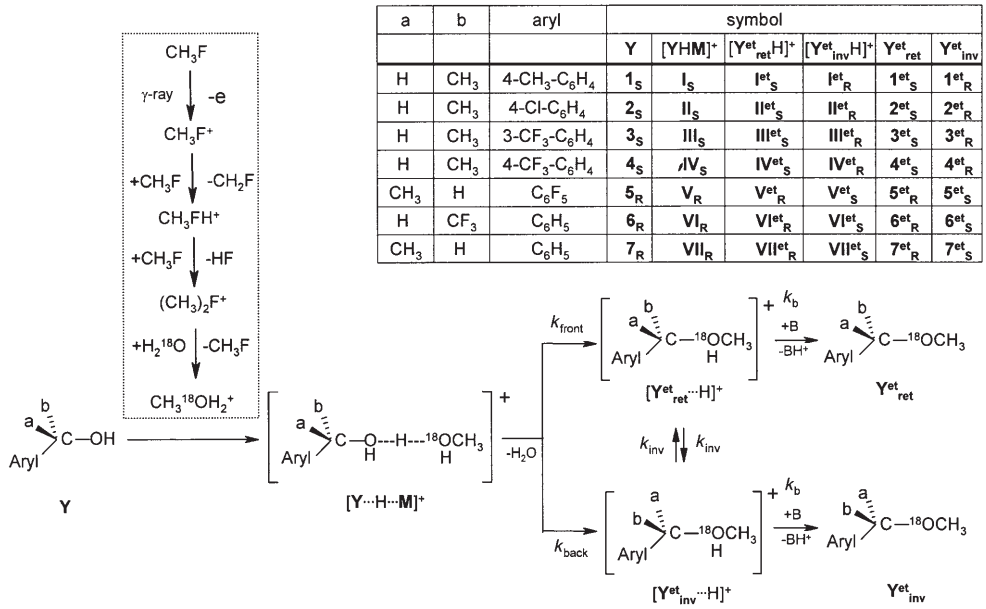

a	b	aryl	symbol					
			Y	$[YHM]^+$	$[Y^{et}_{ret}H]^+$	$[Y^{et}_{inv}H]^+$	Y^{et}_{ret}	Y^{et}_{inv}
H	CH_3	4-CH_3-C_6H_4	$\mathbf{1}_S$	$\mathbf{I}_S$	$\mathbf{I}^{et}{}_S$	$\mathbf{I}^{et}{}_R$	$\mathbf{1}^{et}{}_S$	$\mathbf{1}^{et}{}_R$
H	CH_3	4-Cl-C_6H_4	$\mathbf{2}_S$	$\mathbf{II}_S$	$\mathbf{II}^{et}{}_S$	$\mathbf{II}^{et}{}_R$	$\mathbf{2}^{et}{}_S$	$\mathbf{2}^{et}{}_R$
H	CH_3	3-CF_3-C_6H_4	$\mathbf{3}_S$	$\mathbf{III}_S$	$\mathbf{III}^{et}{}_S$	$\mathbf{III}^{et}{}_R$	$\mathbf{3}^{et}{}_S$	$\mathbf{3}^{et}{}_R$
H	CH_3	4-CF_3-C_6H_4	$\mathbf{4}_S$	$\mathbf{IV}_S$	$\mathbf{IV}^{et}{}_S$	$\mathbf{IV}^{et}{}_R$	$\mathbf{4}^{et}{}_S$	$\mathbf{4}^{et}{}_R$
CH_3	H	C_6F_5	$\mathbf{5}_R$	$\mathbf{V}_R$	$\mathbf{V}^{et}{}_R$	$\mathbf{V}^{et}{}_S$	$\mathbf{5}^{et}{}_R$	$\mathbf{5}^{et}{}_S$
H	CF_3	C_6H_5	$\mathbf{6}_R$	$\mathbf{VI}_R$	$\mathbf{VI}^{et}{}_R$	$\mathbf{VI}^{et}{}_S$	$\mathbf{6}^{et}{}_R$	$\mathbf{6}^{et}{}_S$
CH_3	H	C_6H_5	$\mathbf{7}_R$	$\mathbf{VII}_R$	$\mathbf{VII}^{et}{}_R$	$\mathbf{VII}^{et}{}_S$	$\mathbf{7}^{et}{}_R$	$\mathbf{7}^{et}{}_S$

Scheme 1.

tion. Furthermore, generation of the complex $[\mathbf{Y}\cdots H\cdots\mathbf{M}]^+$ takes place in the absence of neutral solvent molecules, that is, $CH_3{}^{18}OH$. Hence, the formation of ^{18}O-labeled[12] ethers $\mathbf{Y}^{et}{}_{ret}$ and $\mathbf{Y}^{et}{}_{inv}$ of Scheme 1 must be necessarily traced to the *intracomplex* solvolysis of $[\mathbf{Y}\cdots H\cdots\mathbf{M}]^+$.

Abstract in Italian: *Il meccanismo e la stereochimica della solvolisi intramolecolare in complessi di tipo* $[\mathbf{Y}\cdots H\cdots\mathbf{M}]^+$ *con* $\mathbf{M}=CH_3{}^{18}OH$ *e* $\mathbf{Y}$*=1-ariletanolo [(S)-1-(*para*-tolil)etanolo (*$\mathbf{1}_S$*), (S)-1-(*para*-clorofenil)etanolo (*$\mathbf{2}_S$*), (S)-1-(*meta*-α,α,α-trifluorometilfenil)etanolo (*$\mathbf{3}_S$*), (S)-1-(*para*-α,α,α-trifluorometilfenil)etanolo (*$\mathbf{4}_S$*), (R)-1-(pentafluorofenil)etanolo (*$\mathbf{5}_R$*), (R)-α-(trifluorometil)benzil alcool (*$\mathbf{6}_R$*), and (R)-1-feniletanolo (*$\mathbf{7}_R$*)] sono stati studiati in fase gassosa (*CH_3F; 720 torr) nell'intervallo di temperatura da 25 a 140 °C. La solvolisi in fase gassosa di* $[\mathbf{Y}\cdots H\cdots\mathbf{M}]^+$ *(*$\mathbf{Y}$*=*$\mathbf{2}_S$*, *$\mathbf{3}_S$*, *$\mathbf{4}_S$*, and *$\mathbf{7}_R$*) comporta una estesa racemizzazione al di sopra di una temperatura* $t^{\#}$ *caratteristica per ogni alcool (per esempio, a* $t^{\#}>60$ *°C per* $\mathbf{7}_R$*), mentre al di sotto di tale temperatura, si osserva un limitato eccesso di ritenzione di configurazione. Prevalente ritenzione di configurazione si osserva invece ad ogni temperatura (*$25 \leq T \leq 120$ *°C) in* $[\mathbf{Y}\cdots H\cdots\mathbf{M}]^+$ *(*$\mathbf{Y}$*=*$\mathbf{1}_S$*, *$\mathbf{4}_S$*, *$\mathbf{5}_R$*, and *$\mathbf{6}_R$*). Questi risultati indicano che la solvolisi intramolecolare di* $[\mathbf{Y}\cdots H\cdots\mathbf{M}]^+$ *procede tramite la formazione dei corrispondenti intermedi benzilici (*Bz^+*), coordinati elettrostaticamente a molecole di* H_2O *e* $CH_3{}^{18}OH$ *(meccanismo* S_N1*). I risultati in fase gassosa sono discussi alla luce di analoghi dati in soluzione. Si conclude che la stereochimica di reazioni solvolitiche unimolecolari è determinate dal tempo di vita e dalla dinamica delle specie transienti coinvolte e, in soluzione, anche dalla natura e dalla dinamica della cavità del solvente.*

The investigation is now extended to other variously substituted 1-arylethanols in order to elucidate the effect of ring substituents on the kinetics and stereochemistry of the intracomplex solvolysis of the relevant $[\mathbf{Y}\cdots H\cdots\mathbf{M}]^+$ complexes. It is thereby anticipated that our knowledge of the factors governing the dynamics of solvolytic processes in the condensed phase can be extended.

Experimental Section

Materials: Methyl fluoride and oxygen were high-purity gases from UCAR Specialty Gases N.V., used without further purification. $H_2{}^{18}O$ (^{18}O content >97%) and $(C_2H_5)_3N$ were purchased from ICON Services. The racemate of 1-(*para*-tolyl)ethanol (*rac*-**1**) was supplied by Lancaster Co. The racemates of 1-(X-phenyl)ethanols [X=*p*-Cl (*rac*-**2**), *m*-CF_3 (*rac*-**3**), *p*-CF_3 (*rac*-**4**)], the pure *R*- ($\mathbf{5}_R$) and *S* enantiomers of 1-(pentafluorophenyl)ethanol ($\mathbf{5}_S$), the pure *R*- ($\mathbf{6}_R$) and *S* enantiomers of α-(trifluoromethyl)benzyl alcohol ($\mathbf{6}_S$), and the pure *R*- ($\mathbf{7}_R$) and *S* enantiomers of 1-phenylethanol ($\mathbf{7}_S$) (Scheme 1) were purchased from Aldrich Co. The *S* enantiomers of 1-(X-phenyl)ethanols [X=*p*-CH_3 ($\mathbf{1}_S$), *p*-Cl ($\mathbf{2}_S$), *m*-CF_3 ($\mathbf{3}_S$), *p*-CF_3 ($\mathbf{4}_S$)], used as starting substrates, were purified from the corresponding racemates by enantioselective semipreparative HPLC on the following chiral columns: i) $\mathbf{1}_S$: FSC-poly-DACH-METACR, 5 μm, 250×4.0 mm i.d., eluent: *n*-hexane/dichloromethane/1,4-dioxane 70:30:5; flow rate: 1.0 mL min^{-1}; detection by UV (254 nm) and ORD (polarimeter) in series; [$k_1'(-)=2.63$; $\alpha=1.12$; t = 25 °C]; ii) $\mathbf{2}_S$: (*R*,*R*)-Ulmo, 5 μm, 250×4.0 mm i.d., eluent: *n*-hexane/propan-2-ol 99:1; flow rate: 2.0 mL min^{-1}; detection by UV (254 nm) and ORD (polarimeter) in series; [$k_1'(-)=3.85$; $\alpha=1.22$; t = 25 °C]; iii) $\mathbf{3}_S$: (*R*,*R*)-Ulmo, 5 μm, 250×4.0 mm i.d., eluent: *n*-hexane/dichloromethane/1,4-dioxane 90:10:3; flow rate: 1.5 mL min^{-1}; detection by UV (254 nm) and ORD (polarimeter) in series; [$k_1'(-)=2.33$; $\alpha=1.09$; t = 25 °C]; iv) $\mathbf{4}_S$: FSC-poly-DACH-METACR, 5 μm, 250×4.0 mm i.d., eluent: *n*-hexane/dichloromethane/1,4-dioxane 80:20:3; flow rate: 1.0 mL min^{-1}; detection by UV (254 nm) and ORD (polarimeter) in series; [$k_1'(-)=4.79$; $\alpha=1.16$; t = 25 °C]. The enantiomeric purity of the isolated enantiomers was checked by enantioselective HRGC on: i) MEGADEX DACTBS-β (30% 2,3-di-*O*-acetyl-6-*O*-*tert*-butyldimethylsilyl-β-cyclodextrin in OV 1701; 25 m long, 0.25 mm

i.d., $d_f = 0.25\,\mu m$) fused silica column, at $60 < t < 170\,^{\circ}C$, $4\,^{\circ}C\,min^{-1}$; ii) MEGADEX 5 (30% 2,3-di-*O*-methyl-6-*O*-pentyl-β-cyclodextrin in OV 1701; 25 m long, 0.25 mm i.d., $d_f = 0.25\,\mu m$) fused silica column at $t = 125\,^{\circ}C$. The *S*- and *R* enantiomers of 1-(X-phenyl)-1-methoxyethanes [(*S*)/(*R*): X = *p*-CH_3 (**1**$^{et}_S$/**1**$^{et}_R$), *p*-Cl (**2**$^{et}_S$/**2**$^{et}_R$), *m*-CF_3 (**3**$^{et}_S$/**3**$^{et}_R$), *p*-CF_3 (**4**$^{et}_S$/**4**$^{et}_R$), of 1-(pentafluorophenyl)-1-methoxyethane (**5**$^{et}_S$/**5**$^{et}_R$), of 1-(α-(trifluoromethylphenyl)-1-methoxyethane (**6**$^{et}_S$/**6**$^{et}_R$), and of 1-phenyl-1-methoxyethane (**7**$^{et}_S$/**7**$^{et}_R$) were synthesized from the corresponding alcohols by the dimethyl sulfate method.[5] Their identity was verified by IR, ^{1}H NMR spectroscopy, and mass spectrometry.

Procedure: The gaseous mixtures were prepared in a greaseless vacuum line. The starting chiral alcohol (0.2–0.6 Torr), $H_2{}^{18}O$ (2–3 Torr), the radical scavenger O_2 (4 Torr), and the powerful base $B = (C_2H_5)_3N$ (0.2–1.4 Torr; proton affinity (PA) = 234.7 kcal mol^{-1})[13] were introduced into carefully evacuated 130 mL Pyrex bulbs, each equipped with a break-seal tip. The bulbs were filled with CH_3F (720 Torr, at each given temperature), cooled to the liquid-nitrogen temperature, and sealed off. The irradiations were carried out at constant temperatures ranging from 25 to 140 °C with a ^{60}Co source to a dose of 2×10^4 Gy at a rate of 1×10^4 Gy h^{-1}, as determined by a neopentane dosimeter. Control experiments, carried out at doses ranging from 1×10^4 to 1×10^5 Gy, showed that the relative yields of products were largely independent of the dose. The radiolytic products were analyzed by enantioselective HRGC, with a Perkin–Elmer 8700 gas chromatograph equipped with a flame-ionization detector, on the same columns used to analyze the starting alcohols. The products were identified by comparison of their retention volumes with those of authentic standard compounds and their identity confirmed by HRGC-MS, using a Hewlett–Packard 5890 A gas chromatograph in line with a HP 5970 B mass spectrometer. Their yields were determined from the areas of the corresponding eluted peaks, using the internal standard (i.e., benzyl alcohol) method and individual calibration factors to correct for the detector response. Blank experiments were carried out to exclude the occurrence of thermal decomposition and racemization of the starting alcohols as well as of their methylated ethers within the temperature range investigated.

The extent of ^{18}O incorporation into the radiolytic products was determined by HRGC-MS, setting the mass analyzer in the selected ion mode (SIM). The ion fragments corresponding to ^{16}O-$[M-CH_3]^+$ and ^{18}O-$[M-CH_3]^+$ (M^+ = parent ion) were monitored to analyze alcohols **1**–**5** and **7** and their corresponding ethers **1**^{et}–**5**^{et} and **7**^{et}. The ion fragments corresponding to ^{16}O-$[M]^+$ and ^{18}O-$[M]^+$ were monitored to analyze alcohols **6**, while the extent of labeling of its methylated ethers **6**^{et} was measured by using the corresponding ^{16}O-$[M-CF_3]^+$ and ^{18}O-$[M-CF_3]^+$ fragments.

Results

γ Radiolysis of the $CH_3F/H_2{}^{18}O$/alcohol gaseous samples leads to the formation of significant yields of the corresponding ^{16}O-labeled ethers (denoted as $\mathbf{X}^{et}$), together with minor amounts of the relevant ^{18}O isotopomers (denoted as $\mathbf{Y}^{et}$, $[\mathbf{Y}^{et}]/[\mathbf{X}^{et}] \leq 0.09$). The ionic origin of these products is demonstrated by the sharp decrease (over 80%) of their abundance as the $(C_2H_5)_3N$ concentration is quintupled.

Predominance of the retained and inverted ^{16}O-labeled ethers, that is, $\mathbf{X}^{et}{}_{ret}$ and $\mathbf{X}^{et}{}_{inv}$, respectively, is mainly[12] attributed to the direct attack of the $(CH_3)_2F^+$ ions on the aromatic alcohol, while the formation of the corresponding ^{18}O-labeled ethers, that is, $\mathbf{Y}^{et}{}_{ret}$ and $\mathbf{Y}^{et}{}_{inv}$, respectively, is traced to the attack on the same alcohols by the $CH_3{}^{18}OH_2{}^+$ ions ($[H\cdots\mathbf{M}]^+$), generated according to the reaction sequence shown in the left-hand side inset of Scheme 1. The different origin of the ^{16}O- and ^{18}O-labeled ethers is testified by their different enantiomeric distribution. This can be easily appreciated by the large discrepancy between the $[\mathbf{X}^{et}{}_{inv}]/\{[\mathbf{X}^{et}{}_{inv}]+[\mathbf{X}^{et}{}_{ret}]\}$ ratio (α in Table 1) and the homologous $[\mathbf{Y}^{et}{}_{inv}]/\{[\mathbf{Y}^{et}{}_{inv}]+[\mathbf{Y}^{et}{}_{ret}]\} = (1+\beta)^{-1}$ one ($\beta = [\mathbf{Y}^{et}{}_{ret}]/[\mathbf{Y}^{et}{}_{inv}]$; Table 1). According to Scheme 1, the rate-constant ratio k_{front}/k_{back} for the frontside versus backside intracomplex solvolysis of $[\mathbf{Y}\cdots H\cdots\mathbf{M}]^+$ can be expressed by the $\beta = [\mathbf{Y}^{et}{}_{ret}]/[\mathbf{Y}^{et}{}_{inv}]$ ratio, once corrected by the $[\mathbf{Y}^{et}{}_{ret}\cdots H] \leftrightarrow [\mathbf{Y}^{et}{}_{inv}\cdots H]$ interconversion during their lifetime τ. Within the reasonable assumption of a fast neutralization of all the ionic intermediates by the strong base $B = (C_2H_5)_3N$ (proton affinity (PA) = 234.7 kcal mol^{-1})[13] and negligible ^{16}O/^{18}O kinetic isotope effects, the α factor can be taken as representative of the extent of the inversion of configuration of $[\mathbf{X}^{et}{}_{ret}\cdots H]^+$ ($[\mathbf{X}^{et}{}_{ret}\cdots H]^+ \leftrightarrow [\mathbf{X}^{et}{}_{inv}\cdots H]^+$) as well as of $[\mathbf{Y}^{et}{}_{ret}\cdots H]^+$ ($[\mathbf{Y}^{et}{}_{ret}\cdots H]^+ \leftrightarrow [\mathbf{Y}^{et}{}_{inv}\cdots H]^+$)[14] during the relevant ion lifetime $\tau = (k_b[B])^{-1}$.[15] In this case, the β term of Table 1 can be expressed in terms of the α factor as shown in Equation (1).[10,14] Rearrangement of Equation (1) leads to the Equation (2) for the k_{front}/k_{back} ratio, that is, the rate-constant ratio for the frontside versus the backside $CH_3{}^{18}OH$-to-H_2O displacement in complex $[\mathbf{Y}\cdots H\cdots\mathbf{M}]^+$ (Scheme 1).

$$\beta = \frac{[(1-\alpha)k_{front}+\alpha k_{back}]}{[\alpha k_{front}+(1-\alpha)k_{back}]} \quad (1)$$

$$\frac{k_{front}}{k_{back}} = \frac{[(1-\alpha)\beta-\alpha]}{[(1-\alpha)-\beta\alpha]} \quad (2)$$

The k_{front}/k_{back} ratios reported in Table 1[16] represent average values obtained from several separate irradiations carried out under the same experimental conditions, and whose reproducibility is expressed by the uncertainty level quoted.

The temperature dependence of the $\log(k_{front}/k_{back})$ is illustrated in Figures 1 and 2. In Figure 1, the plots relative to $[\mathbf{Y}\cdots H\cdots\mathbf{M}]^+$ ($\mathbf{M}$ = $\mathbf{II}_S$, $\mathbf{III}_S$, or $\mathbf{VII}_R$) are linear below a characteristic temperature $t^{\#}$ (e.g. $t^{\#} < 100\,^{\circ}C$ for $\mathbf{III}_S$). At $t > t^{\#}$, they tend towards a constant value of zero or even negative (i.e., with $\mathbf{VII}_R$). This means that above $t^{\#}$ intracomplex solvolysis of $[\mathbf{Y}\cdots H\cdots\mathbf{M}]^+$ mainly yields the $[\mathbf{Y}^{et}{}_{ret}\cdots H]^+/[\mathbf{Y}^{et}{}_{inv}\cdots H]^+ \approx 1$ racemate, whereas, below $t^{\#}$ the solvolysis of the same complex is appreciably stereoselective and frontside substitution predominates over backside substitution ($[\mathbf{Y}^{et}{}_{ret}\cdots H]^+/[\mathbf{Y}^{et}{}_{inv}\cdots H]^+ > 1$). In contrast, the plots relative to $[\mathbf{Y}\cdots H\cdots\mathbf{M}]^+$ ($\mathbf{M}$ = $\mathbf{I}_S$ (Figure 1) and $\mathbf{IV}_S$, $\mathbf{V}_R$, and $\mathbf{VI}_R$ (Figure 2)) are linear over the entire 25–120 °C temperature range explored and do not exhibit any tendency to reach a plateau within the same temperature interval (except perhaps $\mathbf{IV}_S$). This means that, in these systems and within the temperature range explored, the frontside substitution invariably prevails over the backside displacement ($[\mathbf{Y}^{et}{}_{ret}\cdots H]^+/[\mathbf{Y}^{et}{}_{inv}\cdots H]^+ > 1$). The linear portions of the Arrhenius plots of Figures 1 and 2 obey the Arrhenius equations shown in Table 2. The differential activation parameter relative to the backside versus frontside solvolyses of $[\mathbf{Y}\cdots H\cdots\mathbf{M}]^+$ are

Table 1. Gas-phase intracomplex substitution in the $[\mathbf{Y}\cdots H\cdots\mathbf{M}]^+$ adducts.

System composition [Torr][a]		$T_{reaction}$	τ[b]	Inversion extent[c]	Yield ratio[d]	Rate-constant ratio[e]	
Substrate	$(C_2H_5)_3N$	[°C]	[ns]	α	β	k_{front}/k_{back}	$\log(k_{front}/k_{back})$
$\mathbf{1}_S$, 0.62	1.16	25	22	0.432	1.25	9.93	0.997
$\mathbf{1}_S$, 0.62	1.19	40	23	0.439	1.20	6.85	0.836
$\mathbf{1}_S$, 0.65	1.13	70	26	0.470	1.08	4.13	0.616
$\mathbf{1}_S$, 0.51	1.11	80	27	0.475	1.06	3.79	0.579
$\mathbf{2}_S$, 0.18	0.80	25	32	0.230	1.26	1.54	0.188
$\mathbf{2}_S$, 0.55	0.78	40	35	0.290	1.14	1.37	0.136
$\mathbf{2}_S$, 0.30	0.63	60	47	0.400	1.03	1.16	0.064
$\mathbf{2}_S$, 0.61	0.79	70	39	0.413	1.01	1.06	0.025
$\mathbf{2}_S$, 0.28	0.90	80	35	0.418	1.01	1.06	0.026
$\mathbf{2}_S$, 0.33	0.61	100	55	0.475	1.00	1.00	0.000
$\mathbf{3}_S$, 0.26	0.40	40	71	0.140	2.10	2.94	0.469
$\mathbf{3}_S$, 0.30	0.49	60	62	0.240	1.49	2.22	0.346
$\mathbf{3}_S$, 0.23	0.41	80	78	0.342	1.17	1.66	0.220
$\mathbf{3}_S$, 0.24	0.61	100	56	0.405	1.03	1.17	0.068
$\mathbf{3}_S$, 0.27	0.67	120	54	0.450	1.01	1.10	0.043
$\mathbf{3}_S$, 0.24	0.60	140	64	0.490	1.00	1.00	0.000
$\mathbf{4}_S$, 0.22	0.68	25	40	0.066	3.53	4.62	0.665
$\mathbf{4}_S$, 0.23	0.73	40	39	0.120	2.91	4.58	0.661
$\mathbf{4}_S$, 0.25	0.49	60	62	0.200	1.81	2.85	0.454
$\mathbf{4}_S$, 0.30	0.51	80	63	0.280	1.40	2.22	0.346
$\mathbf{4}_S$, 0.40	0.49	100	70	0.380	1.08	1.38	0.140
$\mathbf{4}_S$, 0.21	0.55	120	66	0.400	1.01	1.05	0.022
$\mathbf{5}_R$, 0.22	0.53	25	52	0.025	7.50	9.25	0.966
$\mathbf{5}_R$, 0.28	0.51	40	57	0.050	5.14	6.97	0.843
$\mathbf{5}_R$, 0.25	0.46	60	67	0.085	3.41	4.85	0.686
$\mathbf{5}_R$, 0.22	0.39	70	81	0.130	2.82	4.61	0.664
$\mathbf{5}_R$, 0.24	0.39	80	85	0.155	2.07	3.04	0.483
$\mathbf{5}_R$, 0.21	0.46	100	75	0.257	1.46	2.25	0.352
$\mathbf{6}_R$, 0.23	0.31	40	89	0.005	36.37	44.50	1.648
$\mathbf{6}_R$, 0.32	0.35	60	86	0.015	16.05	21.22	1.372
$\mathbf{6}_R$, 0.30	0.31	70	99	0.025	13.55	20.72	1.316
$\mathbf{6}_R$, 0.34	0.32	80	99	0.030	9.44	13.29	1.123
$\mathbf{6}_R$, 0.35	0.24	100	141	0.081	4.68	7.82	0.352
$\mathbf{7}_R$, 0.22	1.15	25	22	0.302	1.26	1.82	0.260
$\mathbf{7}_R$, 0.22	1.25	30	20	0.296	1.22	1.63	0.213
$\mathbf{7}_R$, 0.23	1.42	40	19	0.303	1.09	1.25	0.097
$\mathbf{7}_R$, 0.25	1.15	60	24	0.387	1.00	1.00	0.000
$\mathbf{7}_R$, 0.30	1.10	70	26	0.407	0.98	0.90	-0.047
$\mathbf{7}_R$, 0.40	1.16	80	26	0.437	0.98	0.85	-0.070
$\mathbf{7}_R$, 0.21	1.18	100	27	0.442	0.98	0.84	-0.076

[a] CH_3F: 720 Torr, $H_2{}^{18}O$: 2–3 Torr; O_2: 4 Torr. Radiation dose: 2×10^4 Gy (dose rate: 1×10^4 Gy h^{-1}). [b] Reaction time, τ, calculated from the reciprocal of the first-order collision constant between the relevant $[\mathbf{Y}^{et}\cdots H]^+$ intermediate and $(C_2H_5)_3N$ (see text). [c] $\alpha=[\mathbf{X}^{et}{}_{inv}]/\{[\mathbf{X}^{et}{}_{inv}]+[\mathbf{X}^{et}{}_{ret}]\}$; see text and ref. [14]. [d] $\beta=\mathbf{Y}^{et}{}_{ret}/\mathbf{Y}^{et}{}_{inv}$; each value is the average of several determinations, with an uncertainty level of ca. 5%. [e] See text.

given in the same table under the relevant $\Delta\Delta H^{\neq}$ and $\Delta\Delta S^{\neq}$ headings.

Discussion

Recent theoretical and experimental studies demonstrated that the kinetics and the stereochemistry of gas-phase nucleophilic substitutions on protonated alcohols $ROH_2{}^+$ crucially depend upon the stability of the R^+ ion.[10,17] Thus, the more stable is the R moiety in the displacement transition structure (TS), the smaller are both the covalent character of the $[\mathbf{M}\cdots R\cdots OH_2]^+$ interactions and the activation barrier associated with the motion of the nucleophile **M** around $ROH_2{}^+$.[17] It follows that frontside substitution becomes competitive with the classical backside displacement by increasing the R^+ stabilization. With highly stabilized R^+, such as the *tert*-butyl cation, the limiting frontside and backside pathways may merge into the S_N1 mechanism.[10,17]

The stabilization energy of substituted 1-arylethyl cations (Bz^+), relative to *tert*-butyl cation, can be derived from the difference between the proton affinity (PA) of the corresponding alkenes, that is, substituted styrenes and 2-methyl-1-propene (PA = 191.7 kcal mol^{-1}),[13] respectively. On the grounds of a well-established correlation between the basicity data of ring-substituted styrenes and the Brown–Hammett σ^+ substituent constants,[18] it is possible to derive the following stability order for Bz^+: *p*-CH_3 > H > *p*-Cl > *m*-CF_3 > *p*-CF_3 > 2,3,4,5,6-F_5 > α-CF_3.[19,20]

Table 2. Differential Arrhenius parameters for the gas-phase intracomplex substitution in the $[\mathbf{Y}\cdots H\cdots\mathbf{M}]^+$ adducts.

Y	Process $[\mathbf{Y}^{et}{}_{ret}\cdots H]^+\leftarrow[\mathbf{Y}\cdots H\cdots\mathbf{M}]^+\rightarrow[\mathbf{Y}^{et}{}_{inv}\cdots H]^+$	Arrhenius Equation (y=1000/2.303RT)	Corr. coeff. (r^2)	$\Delta\Delta H^{\neq}$[a] [kcal mol^{-1}]	$\Delta\Delta S^{\neq}$[b] [cal mol^{-1} K^{-1}]
$\mathbf{1}_S$	$\mathbf{I}^{et}{}_S\leftarrow\mathbf{I}_S\rightarrow\mathbf{I}^{et}{}_R$	$\log(k_{front}/k_{back})=(-1.6\pm0.1)+(3.4\pm0.6)y$	0.997	3.4±0.6	7.2±0.5
$\mathbf{2}_S$	$\mathbf{II}^{et}{}_S\leftarrow\mathbf{II}_S\rightarrow\mathbf{II}^{et}{}_R$	$\log(k_{front}/k_{back})=(-0.9\pm0.1)+(1.5\pm0.1)y$	0.979	1.5±0.1	4.3±0.4
$\mathbf{3}_S$	$\mathbf{III}^{et}{}_S\leftarrow\mathbf{III}_S\rightarrow\mathbf{III}^{et}{}_R$	$\log(k_{front}/k_{back})=(-2.0\pm0.2)+(3.5\pm0.3)y$	0.989	3.5±0.3	9.1±0.7
$\mathbf{4}_S$	$\mathbf{IV}^{et}{}_S\leftarrow\mathbf{IV}_S\rightarrow\mathbf{IV}^{et}{}_R$	$\log(k_{front}/k_{back})=(-2.1\pm0.2)+(3.9\pm0.4)y$	0.963	3.9±0.4	9.6±1.1
$\mathbf{5}_R$	$\mathbf{V}^{et}{}_R\leftarrow\mathbf{V}_R\rightarrow\mathbf{V}^{et}{}_S$	$\log(k_{front}/k_{back})=(-2.0\pm0.2)+(4.1\pm0.4)y$	0.969	4.1±0.4	9.3±1.2
$\mathbf{6}_R$	$\mathbf{VI}^{et}{}_R\leftarrow\mathbf{VI}_R\rightarrow\mathbf{VI}^{et}{}_S$	$\log(k_{front}/k_{back})=(-2.9\pm0.4)+(6.6\pm0.6)y$	0.977	6.6±0.6	13.5±1.7
$\mathbf{7}_R$	$\mathbf{VII}^{et}{}_R\leftarrow\mathbf{VII}_R\rightarrow\mathbf{VII}^{et}{}_S$	$\log(k_{front}/k_{back})=(-2.2\pm0.3)+(3.4\pm0.4)y$	0.967	3.4±0.4	10.2±1.4

[a] $\Delta\Delta H^{\neq}=\Delta H^{\neq}{}_{back}-\Delta H^{\neq}{}_{front}$. [b] $\Delta\Delta S^{\neq}=\Delta S^{\neq}{}_{back}-\Delta S^{\neq}{}_{front}$.

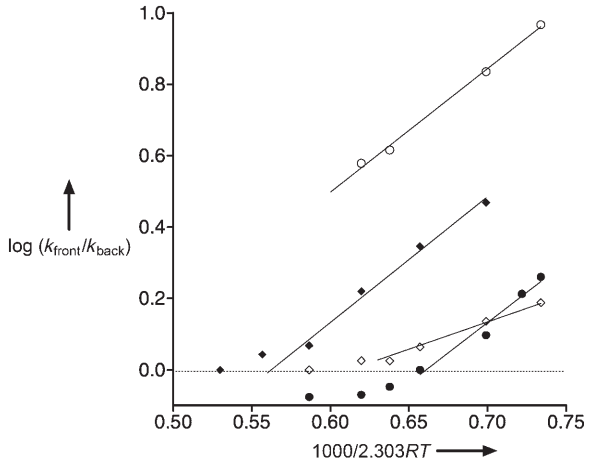

Figure 1. Temperature dependence of the k_{front}/k_{back} ratios for the intracomplex solvolyses of $\mathbf{I}_S$ (○), $\mathbf{II}_S$ (◇), $\mathbf{III}_S$ (◆), and $\mathbf{VII}_R$ (●).

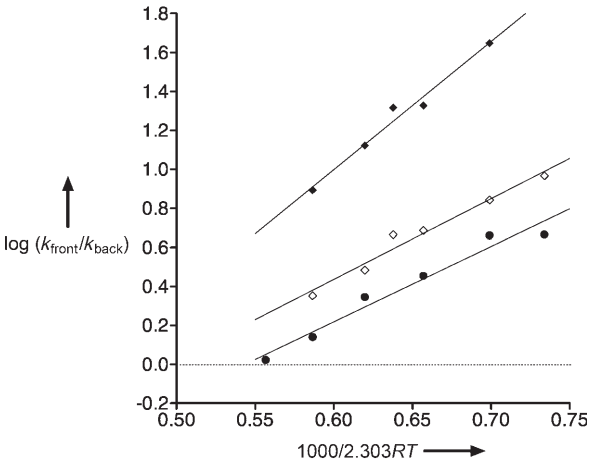

Figure 2. Temperature dependence of the k_{front}/k_{back} ratios for the intracomplex solvolyses of $\mathbf{IV}_S$ (●), $\mathbf{V}_R$ (◇), and $\mathbf{VI}_R$ (◆).

Since most of them are significantly more stable than *tert*-butyl cation, the intracomplex displacement in $[\mathbf{Y}\cdots\mathrm{H}\cdots\mathbf{M}]^+$ is thought to proceed through a S_N1 process involving transition states characterized by noncovalent interactions between Bz^+ and the $CH_3{}^{18}OH/H_2O$ pair and qualitatively resembling the structures depicted in Figure 3. The formation of the relevant $\mathbf{Y}^{et}{}_{ret}/\mathbf{Y}^{et}{}_{inv} \approx 1$ racemate from $\mathbf{II}_S$, $\mathbf{III}_S$, and $\mathbf{VII}_R$ above the corresponding $t^{\#}$, is entirely consistent with this view. The S_N1 model may also account for the predominance of $\mathbf{Y}^{et}{}_{ret}$ over $\mathbf{Y}^{et}{}_{inv}$ from $\mathbf{I}_S$, $\mathbf{IV}_S$, $\mathbf{V}_R$, and $\mathbf{VI}_R$, at all temperatures, and from $\mathbf{II}_S$, $\mathbf{III}_S$, and $\mathbf{VII}_R$, below $t^{\#}$, under the assumption of a hindered motion of $CH_3{}^{18}OH$ around the Bz^+ moiety in the relevant TS before covalent bonding.[10]

Indeed, the procedure adopted to produce $[\mathbf{Y}\cdots\mathrm{H}\cdots\mathbf{M}]^+$ in the gas phase requires that the $CH_3{}^{18}OH$ moiety is generated in the same region of space containing the leaving H_2O molecule and is originally proton-bonded to it (Scheme 1). With this arrangement, frontside attack of $CH_3{}^{18}OH$ on Bz^+ may be favoured by the predominant local concentration of

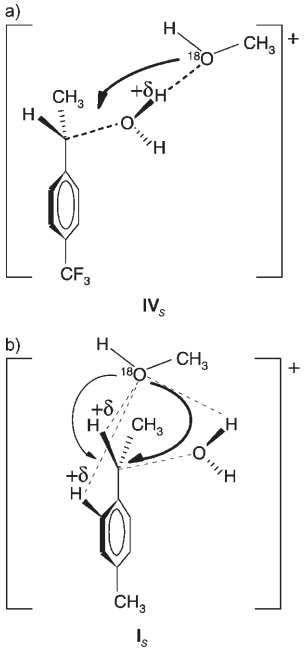

Figure 3. Schematic representation of the evolution of the reactive intermediates involved in the intracomplex nucleophilic substitution in a) $[\mathbf{Y}\cdots\mathrm{H}\cdots\mathbf{M}]^+$ ($\mathbf{Y}=\mathbf{III}_S$, $\mathbf{IV}_S$, $\mathbf{V}_R$, and $\mathbf{VI}_R$) and b) $[\mathbf{Y}\cdots\mathrm{H}\cdots\mathbf{M}]^+$ ($\mathbf{Y}=\mathbf{I}_S$, $\mathbf{II}_S$, and $\mathbf{VII}_R$).

the nucleophile on the same prochiral face of Bz^+ wherefrom the leaving group is released. This is a special case of substrate-directable reactions,[21] called *troposelective* substitution.[22] The preferred frontside attack of $CH_3{}^{18}OH$ on Bz^+ in $[\mathbf{Y}\cdots\mathrm{H}\cdots\mathbf{M}]^+$ is always accompanied by a variable extent of backside substitution, consequently proceeding through the relocation of the $CH_3{}^{18}OH$ on the opposite face of Bz^+. According to previous computational and experimental evidence,[23] the TS for such a facial relocation involves significant electrostatic interactions between the O atom of the nucleophile and the acidic α (H_α) and, if available, *ortho* (H_{ortho}) hydrogen atoms of Bz^+. If Bz^+ contains strong electron-withdrawing substituents (EWG), the interaction with H_α prevails over that with H_{ortho}.

Gas-phase intracomplex nucleophilic displacement in $[\mathbf{Y}\cdots\mathrm{H}\cdots\mathbf{M}]^+$ is expected to be facilitated by charge dispersal over all moieties involved in the relevant TS. Free Bz^+ transients during intracomplex displacement are destabilized by strong EW groups, such as α-CF_3, *m*-CF_3 ($\sigma^+=+0.52$), *p*-CF_3 ($\sigma^+=+0.61$), or five-ring F atoms. The charge prefers to reside as far as possible from ring EW groups. Consequently the leaving H_2O moiety efficiently interacts with the incipient Bz^+ and, therefore, can maintain a strong hydrogen-bond (HB) interaction with the $CH_3{}^{18}OH$ nucleophile as well (dashed line in Figure 3a). The result is that the $CH_3{}^{18}OH$ nucleophile is kept away from the H_α atom of the incipient Bz^+ during the C_α–O bond cleavage. With this arrangement, frontside attack of the nucleophile on Bz^+ is strongly favored, whereas relocation of the $CH_3{}^{18}OH$ on its back face is hindered by the lack of a sufficiently intense $^{18}O\cdots H_\alpha$ interaction. This model is supported by the $\Delta\Delta H^{\neq}$

$= (\Delta H^{\neq}_{back} - \Delta H^{\neq}_{front})$ and $\Delta\Delta S^{\neq} = (\Delta S^{\neq}_{back} - \Delta S^{\neq}_{front})$ terms of Table 2, which express the difference between the activation parameters for face-to-face relocation of $CH_3{}^{18}OH$ in the relevant electrostatic complex versus its frontside addition to the Bz^+ moiety. The relatively large $\Delta\Delta H^{\neq}$ (3.5–6.6 kcal mol^{-1}) and $\Delta\Delta S^{\neq}$ (9.1–13.5 cal mol^{-1} K^{-1}) values, measured for $\mathbf{III}_S$, $\mathbf{IV}_S$, $\mathbf{V}_R$ and $\mathbf{VI}_R$ (Table 2), reflect the relative increase in energy and degrees of freedom when $CH_3{}^{18}OH$ frees itself from the leaving H_2O and moves to the opposite Bz^+ side.

Free Bz^+, containing either weak electron-donating groups (EDG), such as *p*-CH_3 ($\sigma^+ = -0.31$), or weak EWG substituents, such as *p*-Cl ($\sigma^+ = +0.11$)), are instead easily generated in $[\mathbf{Y}\cdots H\cdots\mathbf{M}]^+$. Their incipient formation leads to the development of a partial positive charge at the H_α and ring hydrogens, which therefore can establish intense interactions with the $CH_3{}^{18}OH$ nucleophile.[24] The result is a relatively frozen TS qualitatively resembling the structure shown in Figure 3b, where the $CH_3{}^{18}OH$ nucleophile is placed between the Bz^+ moiety and the leaving H_2O, in a position still favouring frontside attack. Obviously, such a facial preference depends critically on the HB strength between the nucleophile and H_2O. At temperatures below $t^{\#}$, HB is strong enough to favour the frontside attack over the backside one. At temperatures above $t^{\#}$, hydrogen bonds are so weakened that they allow the nucleophile to attack both faces of Bz^+ with almost equal probability ($\mathbf{Y}^{et}_{ret}/\mathbf{Y}^{et}_{inv} \approx 1$; Figure 1). Again, this model is supported by the differential $\Delta\Delta H^{\neq}$ and $\Delta\Delta S^{\neq}$ parameters, measured for $\mathbf{I}_S$, and $\mathbf{II}_S$, respectively (Table 2). Their relatively small values ($\Delta\Delta H^{\neq} =$ 1.5–3.4 kcal mol^{-1}; $\Delta\Delta S^{\neq} =$ 4.3–7.2 cal mol^{-1} K^{-1}) reflect the limited surplus in activation energy and degrees of freedom for the motion of the $CH_3{}^{18}OH$ nucleophile from the front to the back of Bz^+. The $\mathbf{VII}_R$ complex behaves somewhat differently, since it exhibits a similarly small $\Delta\Delta H^{\neq}$ value (3.4 ± 0.4 kcal mol^{-1}), but accompanied by a more pronounced $\Delta\Delta S^{\neq}$ value (10.2 ± 1.4 cal mol^{-1} K^{-1}). A plausible explanation for these findings may be found in the hypothesis of a tighter $C_\alpha\cdots OH_2$ interaction in the relevant TS, which makes the frontside $CH_3{}^{18}OH$ attack entropically less favored since encumbered by the presence of the leaving molecule in the neighbour of the reaction center. This interpretation may also explain the slightly predominant inversion of configuration, observed for $\mathbf{VII}_R$ at $t > t^{\#}$ ($\mathbf{Y}^{et}_{ret}/\mathbf{Y}^{et}_{inv} < 1$; Figure 1).

Comparison with related solution data: The above gas-phase reaction pathway may represent a guideline for understanding the effects of the presence and the nature of the solvent cage on the mechanism and the stereochemistry of 1-arylethanol solvolysis in solution. The S_N1 mechanism of gas-phase 1-arylethanol solvolysis, involving predominant retention of configuration, finds an interesting correspondence in the same process carried out in electrophilic solvents, such as phenol.[25] Indeed, in phenol solutions, 1-arylethanols undergo retentive phenolysis to an extent which depends on the electronic properties of their ring substituents. These findings have been interpreted in terms of a mechanism involving the intimate four-center ion-pair intermediate, shown in Figure 4a. Here, the phenol molecule electrophilically assists the departure of the leaving group OH^- before frontside attack by the incipient PhO^- ion on the Bz^+ residue (another case of troposelective substitution). In our gas-phase systems, the role of phenol is taken over by the $CH_3{}^{18}OH_2{}^+$ ion which assists the release of the leaving group OH^- before frontside attack by the $CH_3{}^{18}OH$ nucleophile on Bz^+ (Figure 4b). The solution and gas-phase models differ in the origin of the minor inverted products. As pointed out above, the inverted $\mathbf{Y}^{et}_{ret}$ products in the gas phase arise from the intracomplex motion of $CH_3{}^{18}OH$ around the Bz^+ moiety (Figure 3). In solution, the same motion is prevented by fast covalent bonding of the Bz^+/PhO^- pair. In other words, it is the long lifetime of the $Bz^+/CH_3{}^{18}OH$ pair in the gas-phase complexes of Figure 3 which determines the yield of the inverted $\mathbf{Y}^{et}_{ret}$ products. In phenolic solution, the formation of the inverted product is instead assigned to: 1) the partial racemization of the intimate Bz^+/OH^- pair first formed in the phenol cage, and 2) the backside attack on the Bz^+/OH^- pair by a PhOH molecule from the solvent cage. Analogous events are obviously prevented in the gas phase. Hence, in phenol, it is the lifetime of the intimate Bz^+/OH^- pair which determines the extent of the inversion of configuration. This conclusion is supported by the pronounced dependence of the phenolysis stereochemistry upon the presence of substituent groups in the ring of 1-arylethanols.[24] Indeed, highly retentive phenolysis is observed with substrates, containing strong EW groups (*p*-NO_2; 90.0% net retention), which are relatively reluctant to generate long-lived intimate Bz^+/OH^- pair. Much less retentive phenolysis is instead observed with substrates, containing ED groups (*p*-OCH_3; 16.6% net retention), which can readily form long-lived Bz^+/OH^- pair.

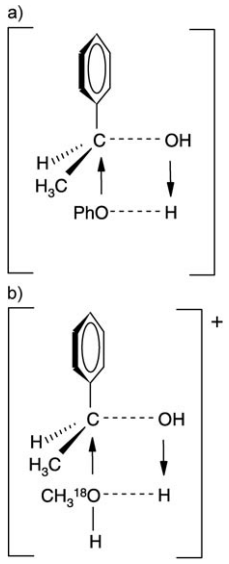

Figure 4. Schematic representation of the evolution of the reactive intermediates involved in the troposelective nucleophilic substitution in the phenolysis of 1-arylethanols a) in solution and b) in the analogous process in gaseous $[\mathbf{Y}\cdots H\cdots\mathbf{M}]^+$ ($\mathbf{Y}$ = 1-arylethanols; $\mathbf{M} = CH_3{}^{18}OH$).

The occurrence of the intimate four-center ion-pair intermediate, depicted in Figure 4a, crucially depends on the nature of the solvent cage. In diluted aqueous acids containing ^{18}O-enriched 1-arylethanols, electrophilic assistance to the leaving $^{18}OH^-$ group is provided by H_3O^+ (*O* denotes the oxygen atom belonging to the acid catalyst) and the mechanistic model is much more similar to that depicted in Figure 3b than in Figure 4a.[26–28] Thus, in these media, ^{18}O-enriched 1-arylethanols reversibly dissociate to correspond-

ing intimate $Bz^+/H_2{}^{18}O/H_2O$ three-body complexes, which are very long-lived because of the low nucleophilicity of water, relative to for example, PhO^-. Within the solvent (H_2O) cage, the $H_2{}^{18}O$ and H_2O are readily interchangeable and moving around Bz^+ at a rate which is comparable with those of the H_2O-to-$H_2{}^{18}O$ and H_2O-to-H_2O exchanges. The consequence is that ^{18}O-enriched 1-phenylalkanols undergo loss of the ^{18}O label with partial racemization (cf. Figure 3b) and inversion of configuration without ^{18}O loss.

The present results provide further support that pure S_N1 processes may follow completely different or even opposite stereochemistry, depending upon the dynamics and the lifetime of the reactive intermediates involved.[10] These factors do not reflect only the kind of interactions operative in the reaction intermediates, but also the nature of the medium in which they are generated. In electrophilic solvents (e.g. PhOH), the S_N1 ion-pair intermediates are short-lived and predominant retention of configuration is observed. In water, the S_N1 ion-pair intermediates are long-lived and extensive racemization takes place. Sometimes, inversion of configuration is observed even for pure S_N1 solvolyses. This may happen when the leaving group hampers the approach of the nucleophile from the frontside (cf. gaseous $[\mathbf{Y}\cdots H\cdots\mathbf{M}]^+$ ($\mathbf{M}=\mathbf{VII}_R$) at $t>t^{\#}$).

Acknowledgements

The work was supported by the Ministero della Università e della Ricerca Scientifica e Tecnologica (MURST-COFIN) and the Consiglio Nazionale delle Ricerche (CNR).

[1] E. D. Hughes, C. K. Ingold, *J. Chem. Soc.* **1935**, 244.
[2] S. Winstein, E. Clippinger, A. H. Feinberg, R. Heck, G. C. Robinson, *J. Am. Chem. Soc.* **1956**, *78*, 328.
[3] J. March, *Advanced Organic Chemistry*, Wiley, New York, **1985**.
[4] I. Dostrovsky, E. D. Hughes, C. K. Ingold, *J. Chem. Soc.* **1946**, 173.
[5] T. W. Bentley, C. T. Bowen, W. Parker, C. I. F. Watt, *J. Am. Chem. Soc.* **1979**, *101*, 2486.
[6] W. P. Jencks, *Chem. Soc. Rev.* **1982**, *11*, 345.
[7] a) T. W. Bentley, C. T. Bowen, D. H. Morten, P. v. R. Schleyer, *J. Am. Chem. Soc.* **1981**, *103*, 5466; b) T. W. Bentley, C. T. Bowen, *J. Chem. Soc. Perkin Trans. 2* **1978**, 557.
[8] J. Dale, *J. Chem. Educ.* **1998**, *75*, 1482.
[9] See, for instance: J. Bromilow, J. L. M. Abboud, C. B. Lebrilla, R. W. Taft, G. Scorrano, V. Lucchini, *J. Am. Chem. Soc.* **1981**, *103*, 5448.
[10] A. Filippi, M. Speranza, *J. Am. Chem. Soc.* **2001**, *123*, 6077.
[11] All elementary steps of the reaction sequence to the $CH_3{}^{18}OH_2{}^+$ (left-hand side inset, Scheme 1) are highly efficient (cf. R. J. Blint, T. B. McMahon, J. L. Beauchamp, *J. Am. Chem. Soc.* **1974**, *96*, 1269; A. Troiani, A. Filippi, M. Speranza, *Chem. Eur. J.* **1997**, *3*, 2063).
[12] The irradiated systems invariably contain $H_2{}^{16}O$, as ubiquitous impurity either initially introduced in the mixture together with its bulk component or formed from its radiolysis. As pointed out previously (cf. A. Troiani, F. Gasparrini, F. Grandinetti, M. Speranza, *J. Am. Chem. Soc.* **1997**, *119*, 4525; M. Speranza, A. Troiani, *J. Org. Chem.* **1998**, *63*, 1020), the average stationary concentration of $H_2{}^{16}O$ in the radiolytic systems is estimated to approach that of the added $H_2{}^{18}O$ (ca. 2–3 Torr). The consequence is that ^{16}O-labeled ethers may as well arise from the attack on the aromatic alcohol by $CH_3{}^{16}OH_2{}^+$, originated by the efficient $(CH_3)_2F^+$ methylation of the ubiquitous $H_2{}^{16}O$. However, given the comparable concentrations of $H_2{}^{16}O$ and $H_2{}^{18}O$ in the irradiated systems, the contribution of this route to the ^{16}O-labeled ethers should approximately parallel that to the ^{18}O-labeled ethers from $CH_3{}^{18}OH_2{}^+$ ($\leq 4\,\%$) and, therefore, be absolutely negligible relative to that involving the direct attack of the $(CH_3)_2F^+$ ions on the alcoholic substrate. The alternative hypothesis that the ^{16}O-labeled ethers may arise from the attack of the aromatic alcohol on $CH_3{}^{18}OH_2{}^+$ and $CH_3{}^{16}OH_2{}^+$ with loss of $H_2{}^{18}O$ and $H_2{}^{16}O$, respectively, can be safely excluded on the ground of the much faster exothermic proton transfer from methanol to the aromatic substrate (e.g. PA(**7**) $\approx 194\,kcal\,mol^{-1}$; PA(methanol) $= 180.3\,kcal\,mol^{-1}$) (ref. [13]).
[13] S. G. Lias, E. P. L. Hunter, *J. Phys. Chem. Ref. Data* **1998**, *27*, 413.
[14] A. Filippi, M. Speranza, *ChemPhysChem* **2004**, *5*, 1540. As pointed out in this reference, such an extensive statement is acceptable only when the α and the β terms are measured in the same gaseous medium. In fact, it has been demonstrated that the extent of the $[\mathbf{X}^{et}{}_{ret}\cdots H]^+\leftrightarrow[\mathbf{X}^{et}{}_{inv}\cdots H]$ (and $[\mathbf{Y}^{et}{}_{ret}\cdots H]^+\leftrightarrow[\mathbf{Y}^{et}{}_{inv}\cdots H]$) rearrangement depends critically on the resonant energy transfer from the discrete vibrational levels of the bulk gas and the $[\mathbf{X}^{et}{}_{ret}\cdots H]^+$ (and $[\mathbf{Y}^{et}{}_{ret}\cdots H]^+$) critical mode active in the inversion transition structure.
[15] The collision constant k_b between the ions of Scheme 1 and $(C_2H_5)_3N$ is calculated according to T. Su, W. J. Chesnavitch, *J. Chem. Phys.* **1982**, *76*, 5183.
[16] The kinetic results concerning the gas-phase solvolysis of $\mathbf{V}_R$ and $\mathbf{VII}_R$ are somewhat different from those reported in ref. [10]. The reason for such a discrepancy is due to the different α factors, applied to correct the measured β terms for the $[\mathbf{Y}^{et}{}_{ret}\cdots H]^+\leftrightarrow[\mathbf{Y}^{et}{}_{inv}\cdots H]$ interconversion. Indeed, in ref. [10], the extent of the $[\mathbf{Y}^{et}{}_{ret}\cdots H]^+\leftrightarrow[\mathbf{Y}^{et}{}_{inv}\cdots H]$ racemization was measured in CH_3Cl, as the bulk gas, whereas the bulk CH_3F is used in the present study. As pointed out, in ref. [14] the extent of the $[\mathbf{Y}^{et}{}_{ret}\cdots H]^+\leftrightarrow[\mathbf{Y}^{et}{}_{inv}\cdots H]$ process depends critically on the resonant energy transfer from the discrete vibrational levels of the bulk gas and the $[\mathbf{Y}^{et}{}_{ret}\cdots H]^+$ critical mode active in the inversion transition structure.
[17] E. Uggerud, L. Bache-Andreassen, *Chem. Eur. J.* **1999**, *5*, 1917.
[18] H. C. Brown, Y. Okamoto, *J. Am. Chem. Soc.* **1958**, *80*, 4979.
[19] A. G. Harrison, R. Houriet, T. T. Tidwell, *J. Org. Chem.* **1984**, *49*, 1302.
[20] F. Marcuzzi, G. Modena, C. Paradisi, C. Giancaspro, M. Speranza, *J. Org. Chem.* **1985**, *50*, 4973.
[21] A. H. Hoveyda, D. A. Evans, G. C. Fu, *Chem. Rev.* **1993**, *93*, 1307.
[22] The term "troposelective" has been coined in ref. [9] by combining the Greek word τροπός (turning)and the Latin word "selectu(m)" from the verb "seligere" (to select).
[23] A. Filippi, M. Speranza, *Chem. Eur. J.* **2003**, *9*, 5274.
[24] According to Figure 3b, weak EWG and EDG substituents promote some coordination of the $CH_3{}^{18}OH$ moiety with the H_α and H_{ortho} of Bz^+. This coordination may explain the lack of any correlation between the differential activation parameters of Table 2 and any simple combinations of field/inductive and resonance effects of the substituents (cf. C. Hansch, A. Leo, R. W. Taft, *Chem. Rev.* **1991**, *91*, 165). Indeed, the ring substituent may exert its effects toward the H_α and H_{ortho} interaction sites to a different, hardly predictable extent.
[25] K. Okamoto, T. Kinoshita, Y. Takemura, H. Yoneda, *J. Chem. Soc. Perkin Trans. 2* **1975**, 1426.
[26] E. Grunwald, A. Heller, F. S. Klein, *J. Chem. Soc.* **1957**, 2604.
[27] M. V. Merritt, S. J. Bell, H. J. Cheon, J. A. Darlington, T. L. Dugger, N. B. Elliott, G. L. Fairbrother, C. S. Melendez, E. V. Smith, P. L. Schwartz, *J. Am. Chem. Soc.* **1990**, *112*, 3560.
[28] M. V. Merritt, D. B. Anderson, K. A. Basu, I. W. Chang, H. J. Cheon, N. E. Mukundan, C. A. Flannery, A. Y. Kim, A. Vaishampayan, D. A. Yens, *J. Am. Chem. Soc.* **1994**, *116*, 5551.

Received: January 16, 2006
Revised: March 27, 2006
Published online: July 14, 2006

